IEEJ Journal of Industry Applications
Vol.9 No.1 pp.36–42 DOI: 10.1541/ieejjia.9.36

Paper

Tension Controller Design Considering Periodic Disturbance Suppression in Roll-to-Roll Web Handling Systems

Kenta Seki[*a)] Senior Member, Takayuki Kikuchi[*] Non-member
Makoto Iwasaki[*] Senior Member

(Manuscript received April 25, 2019, revised Sep. 2, 2019)

This paper presents a modeling and tension controller design approach for web handling systems. In these systems, the web handling technology is a key component in the high-precision manufacturing of web products such as thin films and papers. However, periodic disturbances in the synchronization with the rotational frequencies of the roller deteriorate the tension control performance during web transportation. In this study, the web transportation system is modeled considering the motor control systems and web dynamics including viscoelasticity. Based on the constructed model, resonant filters are designed and used as an additional feedback compensator to shape the sensitivity characteristics for the disturbances. By using the compensator, the sensitivity gain of the tension control system can be reduced at specific frequencies, including the rotational frequencies of the rollers. The effectiveness of the designed tension controller is evaluated by conducting experiments using a prototype of the basic roll-to-roll web handling system.

Keywords: roll-to-roll web handling systems, tension control, periodic disturbance, disturbance suppression, loop-shaping

1. Introduction

Long flexible sheets, such as papers, plastic films, metallic lamina, and flexible panels, are called "webs". Web conversion involves processes that modify the physical properties of the web material, such as coating, printing, drying, and lamination, where the web handling processes consist of those processes associated with web transportation [(1)]. The roll-to-roll web handling system to transport the web typically comprises an unwind/rewind roller, guide rollers, drive rollers coupled onto servo motors, and a processing part. In the system, web tension control plays an important role in improving the quality of the product. To regulate the tension to a constant value, a tension feedback control system is generally designed based on the detected tension signal using load cells or the dancer roller as a measurement device [(2)]. PI or PID controllers are generally used for the tension controller, and they consider tracking performance and system stability. In addition, advanced controllers have been proposed, e.g., PID control with variable gains [(3)], observer-based tention feedback control [(4)], robust control [(5)(6)], and a back-stepping controller [(7)]. These approaches have obtained good tracking performance for the tension reference in the simple web handling systems. In contrast, unacceptable velocity variation causes a detrimental variation in tension. In practice, periodic disturbances owing to the misalignment or eccentricity of rollers act on the tension control system as external disturbances [(8)]. Disturbances with specific frequencies, which synchronize with the rotation frequency of the rollers, interfere with the tension control system. In recent years, it has not been possible to ignore the disturbance effect because higher precise tension control is required, particularly in the growing market of the printed electronics industry [(9)]. Since the misalignment or eccentricity of rollers cannot be inherently removed in the manufacturing process of the rollers and mechanical systems, it is necessary to compensate for the effect in some way. From the mechanical design point of view, the aerostatic bearing rollers have been developed to reduce the machining and assembly errors of the rollers [(10)]. Flexure-based precision roll-to-roll machine has been also developed to reduce the effect of the disturbance, where the position of roller shaft is directly calibrated through the flexure mechanisms driven by voice coil and stepper motors [(11)]. Since the flexure mechanisms possess nanometer level repeatability, it is possible to compensate for the tension error with high accuracy. On the other hand, it is also required that the effect of disturbance is compensated by controller design approach as well as the improvement of mechanism.

This paper presents a controller design considering periodic disturbance suppression owing to the eccentricity of the rollers in the roll-to-roll web handling system. A loop-shaping technique considering sensitivity reduction is an effective and practical approach. To reduce the sensitivity gains of the control system at specific frequencies, resonant filters are added to the existing controller [(12)]. This add-on controller has an advantage of practicality because the filters are easily added by the number of corresponding disturbance frequencies. Before consideration of the resonant filter design, the roll-to-roll web handling system is modeled considering the motor control systems and web dynamics because the design procedure is based on the open-loop characteristic. In the modeling, the viscoelasticity of the web, in particular,

a) Correspondence to: Kenta Seki. E-mail: k-seki@nitech.ac.jp
* Department of Electrical and Mechanical Engineering, Nagoya Institute of Technology
Gokiso, Showa, Nagoya, Aichi 466-8555, Japan

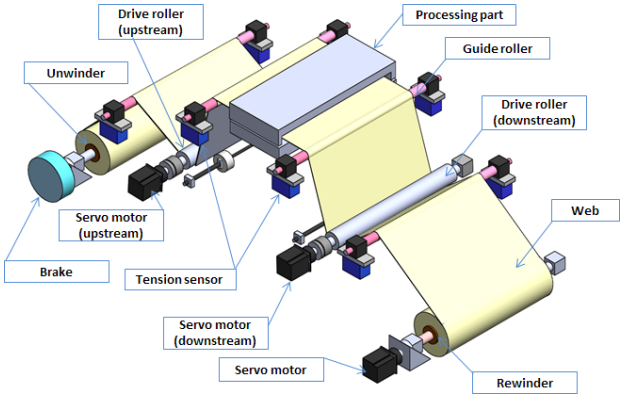

Fig. 1. Schematic overview of the target roll-to-roll web handling system

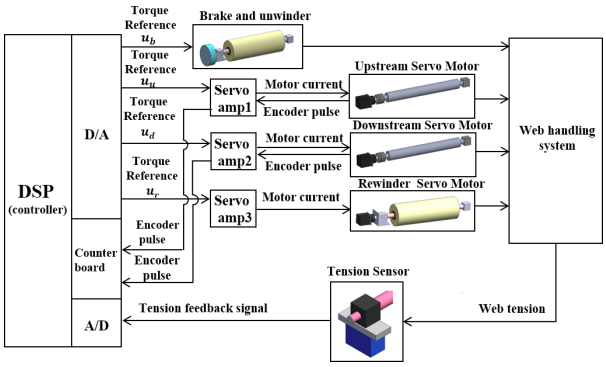

Fig. 2. System configuration of the target roll-to-roll web handling system

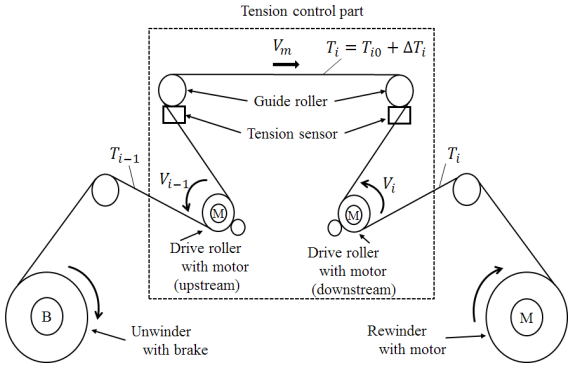

Fig. 3. Schematic view of tension control part in the roll-to-roll web handling system

should be considered to accurately reproduce the dynamics in a higher frequency range. On the basis of the constructed model, resonant filters are designed to reduce the sensitivity gain at specific frequencies including the rotational frequencies of the rollers. In addition, the frequency is updated by calculating the diameter change during winding of the web. The effectiveness of the designed tension control system is verified by conducting experiments using a prototype of a basic roll-to-roll web handling system.

2. Target Roll-to-Roll Web Handling System

Figure 1 shows a schematic overview of the target roll-to-roll web handling system, where the system is a simple configuration by which various problems can be evaluated. The system consists of an unwinder, a rewinder, servo motors, guide/drive rollers, and tension sensors. Initial web tension is uniformly regulated by the servo motor and the brake system connected to the rewinder and unwinder, respectively. The drive rollers are controlled by the servo motors through the shaft, and are set on both sides of the processing part. The transportation velocity of the web is determined by the rotational velocities of both servo motors connected to the drive rollers. In addition, the web tension at the processing part is controlled using the velocity difference between the drive rollers of the upstream and downstream sides. The tension at the processing part is detected by the tension sensors attached to the guide rollers.

Figure 2 shows the system configuration of the target roll-to-roll web handling system. The torque of the servo motor of the rewinder and the brake of the unwinder are controlled based on the current signals. The velocity control system is constructed for the upstream and downstream servo motors based on the encoder pulse. The bandwidth of the velocity control loop is set at ten times higher than that of the tension control loop. The tension signal is transferred to a controller (digital signal processor: DSP) through a sensor amplifier with a sampling period of 0.5 ms. Drive voltages to the servo motors are provided through a servo amplifier based on each reference calculated by the controller.

3. Modeling and Basic Tension Control System

3.1 Basic Model of Web Dynamics The web dynamics are mathematically modeled to design the tension controller based on the model. Figure 3 shows the schematic view of the tension control part, where the V_m indicates steady transportation velocity of the web, V_{i-1} indicates the peripheral velocity of the upstream drive roller, V_i indicates the peripheral velocity of the downstream drive roller, T_i indicates the web tension between the drive rollers, T_{i0} indicates the initial tension between the drive rollers, T_{i-1} indicates the web tension before the upstream drive roller, T_{i+1} indicates the web tension after the downstream drive roller, and ΔT_i indicates the change in web tension. The equation representing the relationship between ΔT_i and the peripheral velocity of the drive rollers can be expressed as follows [1]:

$$\frac{d}{dt}\Delta T_i(t) = -\frac{V_m}{L_i}\Delta T_i(t) + \frac{V_m}{L_i}\Delta T_{i-1}(t) + \frac{AE}{L_i}(V_i(t) - V_{i-1}(t)), \cdots\cdots\cdots\cdots (1)$$

where A indicates the cross-sectional area of the web, E indicates the Young's modulus of the web, L_i indicates the distance between the drive rollers, and ΔT_{i-1} indicates the change of tension. In $\Delta T_{i-1} = 0$, the transfer function $P_w(s)$ from difference in peripheral velocity to ΔT_i can be derived as follows:

$$P_w(s) = \frac{\Delta T_i(s)}{V_i(s) - V_{i-1}(s)} = \frac{AE}{L_i s + V_m}. \cdots\cdots\cdots\cdots (2)$$

3.2 Web Dynamics Considering Viscoelasticity Web dynamics exist in resonant vibrations which are caused by the viscoelasticity of the web. Figure 4 shows the dynamic

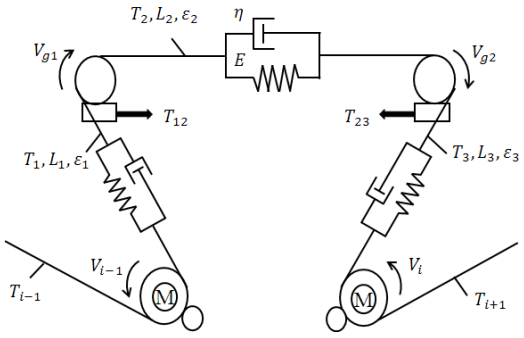

Fig. 4. Dynamic model considering viscoelasticity between two consecutive rollers

model of the tension control part considering viscoelasticity of the web between two consecutive rollers. For the viscoelasticity of the web, the Voigt model is used as the lumped parameter model of the material. In the figure, η and ε indicate the viscosity and strain of the web, respectively. According to the Voigt model, the stress $\sigma_i(t)$ of each part can be expressed as follows:

$$\sigma_i(t) = E\varepsilon_i(t) + \eta\frac{d\varepsilon_i(t)}{dt}. \quad \cdots\cdots (3)$$

The relationship between $\sigma_i(t)$ and $T_i(t)$ is given as follows:

$$T_i(t) = A\sigma_i(t) = A\left(E + \eta\frac{d}{dt}\right)\varepsilon_i(t). \quad \cdots\cdots (4)$$

In addition, the relationship between $\varepsilon(t)$ and the peripheral velocity of the roller V can be given as follows [1]:

$$\frac{d\varepsilon(t)}{dt} = -\frac{V_m}{L_i}\varepsilon(t) + \frac{V_i(t)}{L_i} - \frac{V_{i-1}(t)}{L_i}. \quad \cdots\cdots (5)$$

Equations (4) and (5) are Laplace transformed and following equations can be obtained:

$$T_i(s) = A(E + \eta s)\varepsilon_i(s), \quad \cdots\cdots (6)$$

$$\varepsilon_i(s) = \frac{1}{L_i s + V_m}(V_i(s) - V_{i-1}(s)), \quad \cdots\cdots (7)$$

where s indicates the Laplace operator. By substituting (7) into (6), the transfer functions of the peripheral velocity for tension can be derived as follows:

$$\frac{T_i(s)}{V_i(s) - V_{i-1}(s)} = \frac{A(E + \eta s)}{L_i s + V_m}, \quad \cdots\cdots (8)$$

Based on (8) and Fig. 4, the block diagram of web dynamics considering viscoelasticity can be expressed as Fig. 5, where J_G indicates the inertia of the guide roller, R_D and R_G indicate the radii of the drive and guide rollers, respectively. The feedback signal T is detected by tension sensor. Since the tension sensor detects the horizontal force acting on the guide roller, T is obtained as follows:

$$T = \frac{T_{12} + T_{23}}{2}, \quad \cdots\cdots (9)$$

$$T_{12} = T_2 + \cos\theta_{12}T_1,$$

$$T_{23} = T_2 + \cos\theta_{23}T_3,$$

where θ_{12} and θ_{23} indicate angle of the web at guide rollers. Table 1 lists the parameters of the web dynamics model. Figure 6 shows the frequency responses of the tension signal T

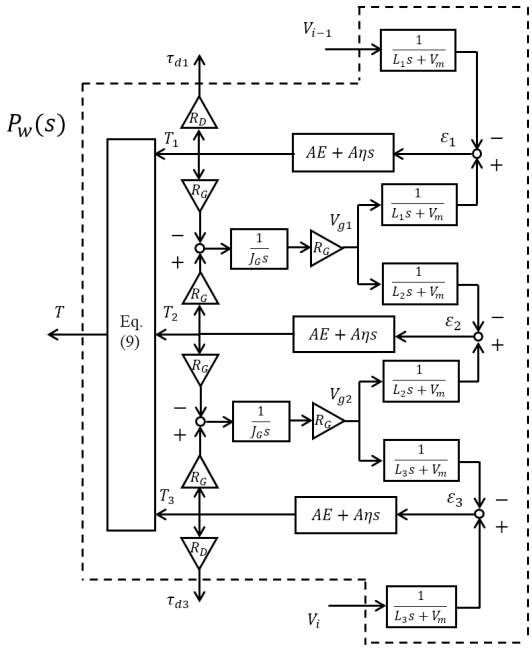

Fig. 5. Block diagram of web dynamics

Table 1. Parameters of the web dynamics model

A [m^2]	1.0×10^{-6}	E [GPa]	2.25	η [MPa·s]	2.81
L_1 [m]	0.6	L_2 [m]	1.22	L_3 [m]	0.6
R_G [m]	0.025	R_D [m]	0.04	θ_{12} [deg]	47.15
J_G [kg·m^2]	2.26×10^{-3}	J_D [kg·m^2]	1.78×10^{-2}	θ_{23} [deg]	47.15

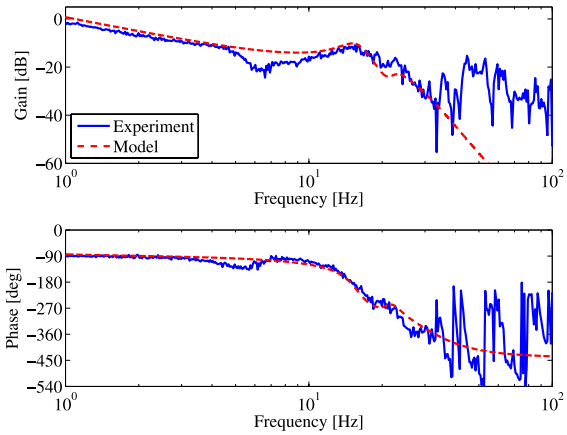

Fig. 6. Frequency responses of web dynamics

for the velocity reference of the upstream roller, where the blue and red lines represent the experimental result and the model as shown in Fig. 5, respectively. In the measurement, swept sinusoidal signal using spectrum analyzer is input to the upstream servo motor under the condition of tension T = 100 N and transportation velocity V_m = 0 m/s. Figure 6 shows that the model considering viscoelasticity of the web can reproduce the resonant frequencies at around 20 Hz.

3.3 Tension Control System Figures 7 and 8 show the block diagrams of motor dynamics and the tension control system, where J_m and J_d represent the inertia of the motor and the drive rollers, respectively; N represents gear ratio, D_g and K_g represent torsional damping and stiffness, respectively; K_{at} represents the gain including the amplifier and

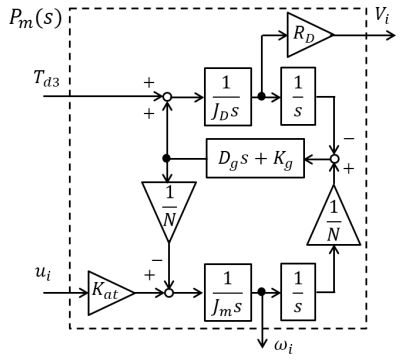

Fig. 7. Block diagram of motor and roller parts

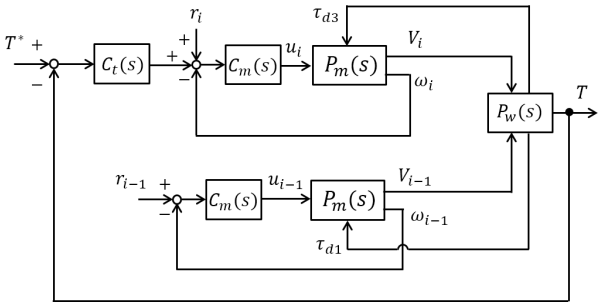

Fig. 8. Basic tension control system

torque constant, u_i represents control input, $C_m(s)$ represents the velocity feedback compensator, $C_t(s)$ represents the tension feedback compensator, ω represents the rotational velocity of the motor, T^* represents the tension reference, and r represents the rotational reference of the motor. To obtain the velocity difference between the drive rollers, the control input (output of tension feedback compensator) is added to the rotational reference of the downstream motor. The reaction force τ_d due to change in tension actually acts on the motor velocity control loop as shown in Fig. 8. The velocity feedback compensator $C_m(s)$ is designed to satisfy the system stability of the motor velocity control loop and the bandwidth of the velocity-loop is set higher than that required for sufficient tension control bandwidth.

The tension feedback compensator $C_t(s)$ is designed as a simple PI compensator, where the parameters are tuned considering system stability and steady state performance. In addition, a notch filter is designed to reduce the gain peak of the resonant frequencies shown in Fig. 6. The transfer function is given as follows:

$$C_t(s) = \left(K_{pt} + \frac{K_{it}}{s}\right) \cdot \frac{s^2 + 2\zeta_{fn}\omega_f + \omega_f^2}{s^2 + 2\zeta_{fd}\omega_f + \omega_f^2} \cdots\cdots\cdots (10)$$

Figure 9 shows the tension response and the frequency analysis result. In the experiment, the rotational reference of the motor is set as 1000 rpm, and initial tension as 100 N. The result shows that the components of specific frequencies appear in the response waveform. The frequencies d_1, d_2, d_3, and d_4 correspond to the rotational frequencies of the unwind roller, drive rollers, guide rollers, and servo motors of the drive rollers, respectively. The disturbance frequencies are different because the diameters of each roller are different.

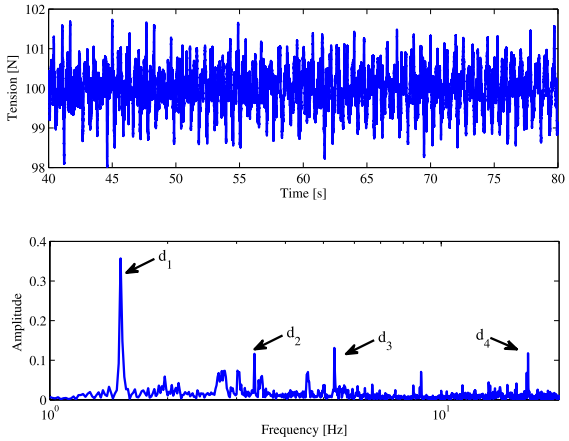

Fig. 9. Tension response and frequency analysis result

In particular, the disturbance frequency of d_1 varies with the diameter of the unwind roller during web feeding. On the other hand, the diameter of rewind roller differs from other rollers. However, the periodic disturbance due to the rewind roller does not appear in Fig. 9 because the eccentricity and misalignment of the roller is smaller than other rollers in this prototype.

4. Design of Resonant Filter

To compensate for the periodic disturbance due to rotational frequencies of the eccentric rollers, a practical disturbance compensation filter is designed to improve the disturbance suppression characteristic at specific frequencies. In this paper, the loop-shaping approach is introduced to shape the sensitivity characteristic of the tension control system. To reduce the sensitivity gains, the vector locus of the open-loop characteristic recedes from the critical point $(-1, 0)$ on the Nyquist diagram [12]. Therefore, the disturbance compensation filter $C_{rf}(s)$ is designed as the following resonant filters with specific frequencies:

$$C_{rf}(s) = \prod_{i=1}^{4} C_{rfi}(s) = \prod_{i=1}^{4} \frac{s^2 + 2\zeta_{ni}\omega_{ni}s + \omega_{ni}^2}{s^2 + 2\zeta_{di}\omega_{di}s + \omega_{di}^2} \cdots\cdots (11)$$

Figure 10 shows open-loop characteristic of tension control system without $C_{rf}(s)$, while Table 2 lists the designed parameters of $C_{rf}(s)$. From the figure, the phase at around the disturbance frequency of d_4 is approximately -180 deg. Although $C_{rf4}(s)$ should have the phase characteristic of $\pm$ 180 deg at the frequency of d_4 to avoid the point $(-1, 0)$ on the Nyquist diagram, the phase of normal resonant filter changes within $\pm$ 90 deg at around resonant frequency. In $C_{rf4}(s)$, therefore, unstable zeros are included to change the phase by -180 deg at resonant frequency. In addition, the phase of frequencies d_1, d_2, and d_3 is approximately -90 deg. The natural frequencies of numerator and denominator are slightly shifted to advance the phase at each resonant frequency in $C_{rf1}(s)$, $C_{rf2}(s)$, and $C_{rf3}(s)$. These parameters are tuned considering the gain reduction at each frequency and maintaining the gain at a higher frequency in the sensitivity characteristic. In Table 2, rotational frequency ω_t changes with the diameter of the unwind roller because the disturbance frequency d_1 depends on the peripheral velocity of the unwind roller.

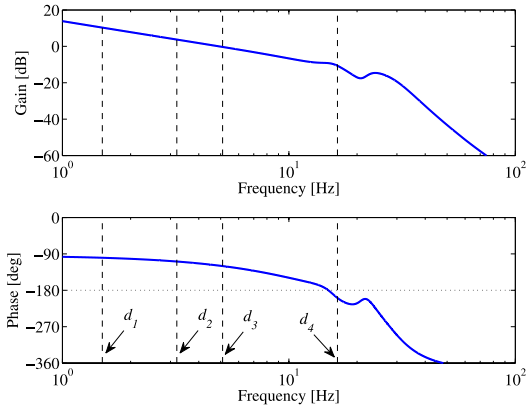

Fig. 10. Open-loop characteristic of tension control system without $C_{rf}(s)$

Table 2. Parameters of $C_{rf}(s)$

i	ζ_{ni}	ζ_{di}	ω_{ni}[rad/s]	ω_{di}[rad/s]
1(C_{rf1})	0.08	0.01	$2\pi\cdot(\omega_t-0.07)$	$2\pi\cdot\omega_t$
2(C_{rf2})	0.02	0.006	$2\pi\cdot 3.2$	$2\pi\cdot 3.33$
3(C_{rf3})	0.015	0.006	$2\pi\cdot 5.1$	$2\pi\cdot 5.33$
4(C_{rf4})	−0.02	0.002	$2\pi\cdot 16.4$	$2\pi\cdot 16.67$

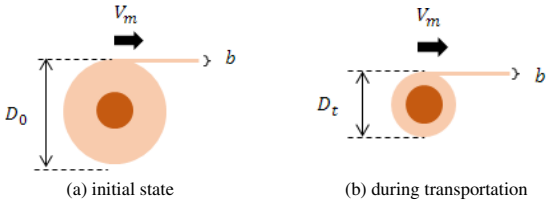

(a) initial state (b) during transportation

Fig. 11. Condition of unwind roller during transportation

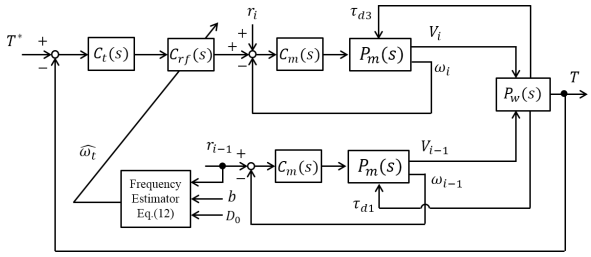

Fig. 12. Tension feedback control system with $C_{rf}(s)$

Figure 11 shows the condition of unwind roller, where D_0 indicates the initial diameter of the roll, D_t indicates the diameter of the unwind roller, and b indicates the thickness of the web. From the figure, ω_t can be updated as the following equation:

$$\omega_t(t) = \frac{V_m}{D_t(t)\cdot\pi}, \quad \cdots\cdots\cdots\cdots\cdots\cdots\cdots\cdots\cdots\cdots \quad (12)$$

$$D_t(t) = \sqrt{D_0^2 - \frac{4\cdot b\cdot V_m}{\pi}t},$$

$$V_m = r_{i-1}\cdot\frac{1}{60}\cdot\frac{1}{N}\cdot 2R_D\cdot\pi,$$

where R_D indicates the radius of the drive roller and N indicates the gear ratio of the servo motor.

Figures 12, 13, 14, and 15 show the block diagram of the tension feedback control system with $C_{rf}(s)$, frequency characteristics of $C_{rf}(s)$, Nyquist diagrams, and sensitivity characteristics, respectively. In Figs. 13, 14, and 15, the

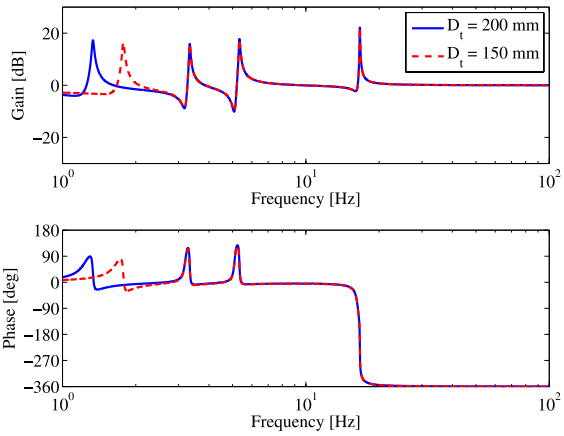

Fig. 13. Frequency characteristics of the $C_{rf}(s)$

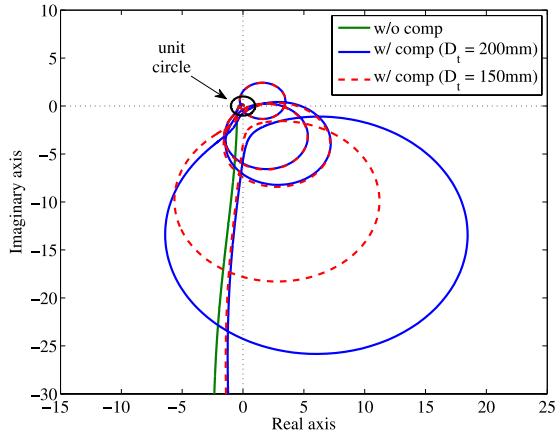

Fig. 14. Nyquist diagrams

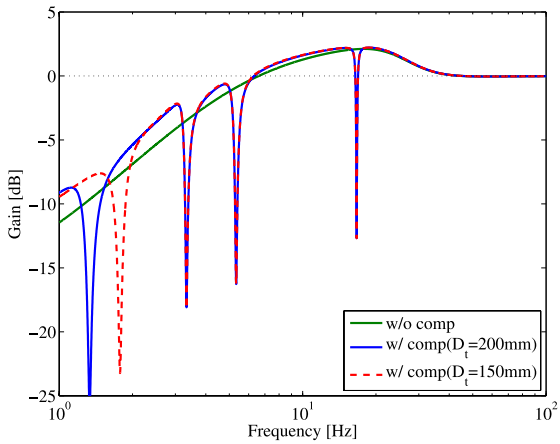

Fig. 15. Sensitivity characteristics

blue and red lines represent the cased of D_t = 200 mm and D_t = 150 mm, respectively. From Fig. 14, the desired vector loci at the resonant frequencies of the filter can be drawn on the right-hand side in the complex plane. As a result, the gain can be sharply reduced at the disturbance frequencies as shown in the sensitivity gains in Fig. 15.

5. Experimental Results

The designed tension control system is verified by conducting experiments using the roll-to-roll web handling system shown in Fig. 1. The experimental conditions are as follows:

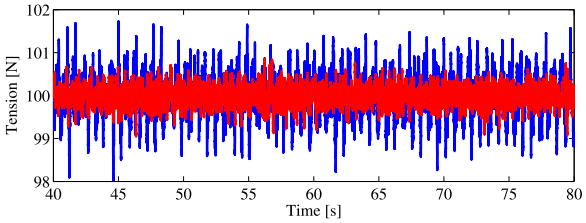

(a) time responses from 40 s to 80 s

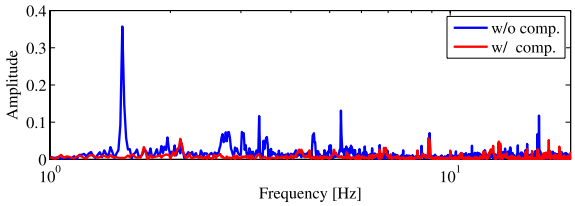

(b) frequency analysis results (time data from 40 s to 60 s)

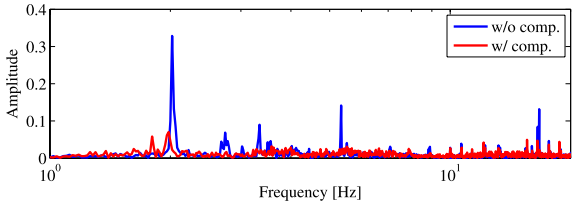

(c) frequency analysis results (time data from 340 s to 360 s)

Fig. 16. Experimental results

- initial tension is set as 100 N,
- rotational velocity of the motor is set as 1000 rpm,
- transportation time is 400 s, and
- diameter of unwind roller changes from 180 mm to 120 mm during experiment.

Figure 16 shows the experimental results, where the red and blue lines represent the result with and without the $C_{rf}(s)$, respectively. In the figure, (a) shows tension responses from 40 s to 60 s, (b) shows the results of frequency analysis using time data from 40 s to 60 s, and (c) shows the results of frequency analysis using time data from 340 s to 360 s. The diameter of unwind roller is approximately 180 mm for (b) and 120 mm for (c), respectively. These results show that the periodic disturbance due to the rotational frequencies of the rollers can be sufficiently suppressed by applying the disturbance compensation filter. From (b) and (c) in the figure, the frequency d_1 clearly changes during web feeding. Therefore, it cannot cope with the frequency change when ω_t is fixed. On the other hand, the disturbance d_1 due to unwind roller can be suppressed by updating the frequency using (12).

6. Conclusions

This paper presented a modeling and a tension controller design approach for roll-to-roll web handling systems. In the system, periodic disturbances in the synchronization with the rotational frequencies of the roller deteriorate the tension control performance during web transportation. Before controller design, the roll-to-roll web handling system was modeled considering the motor control systems and web dynamics. In the modeling, the viscoelasticity of the web was considered to accurately reproduce the dynamics. To compensate for the disturbances, an additional feedback compensator was designed to shape the sensitivity characteristic based on the model of the system. By using the compensator, the sensitivity gain of the tension control system was reduced at specific frequencies, including the rotational frequencies of the rollers. For the disturbance due to the rotation of unwind roller, the frequency was updated by calculating the diameter change during winding of the web. The effectiveness of the designed tension controller was verified by conducting experiments using a prototype of the basic roll-to-roll web handling system.

References

(1) H. Hashimoto: “Theory and application of web handling”, *Converting Technical Institute* (2015)

(2) N.A. Ebler, R. Arnason, G. Michaelis, and N. D’Sa: “Tension control: dancer rolls or load cells”, *IEEE Transactions on Industry Applications*, Vol.29, No.4, pp.727–739 (1993)

(3) K. Reid, K. Shin, and K. Lin: “Variable-Gain Control of Longitudinal Tension in A Web Transport System”, *ASME Applied Mechanical Division*, Vol.149, pp.87–100 (1992)

(4) K.C. Lin: “Observer-Based Tension Feedback Control With Friction and Inertia Compensation”, *IEEE Transactions on Control Systems Technology*, Vol.11, No.1, pp.109–118 (2003)

(5) H. Koç, D. Knittel, M. Mathelin, and G. Abba: “Modeling and Robust Control of Winding Systems for Elastic Webs”, *IEEE Transactions on Control Systems Technology*, Vol.10, No.2, pp.197–208 (2002)

(6) D. Knittel, E. Laroche, D. Gigan, and H. Koç: “Tension Control for Winding Systems With Two degrees-of-Freedom H∞ Controllers”, *IEEE Transactions on Industry Applications*, Vol.39, No.1, pp.113–120 (2003)

(7) K.H. Choi, T.T. Tran, and D.S. Kim: “Back-Stepping Controller Based Web Tension for Roll-to-Roll Web Printed Electronics System”, *Journal of Advanced Mechanical Design, Systems, and Manufacturing*, Vol.5, No.1, pp.7–21 (2011)

(8) K.H. Shin, J.J. Jang, H.K. Kang, and S.H. Song: “Compensation Method for Tension Disturbance Due to an Unknown Roll Shape in a Web Transport System”, *IEEE Transactions on Industry Applications*, Vol.39, No.5, pp.1422–1428 (2003)

(9) N. Kooy, K. Mohamed, L.T. Pin, and O.S. Guan: “A review of roll-to-roll nanoimprint lithography”, *Nanoscale Research Letters*, Vol.9, No.1, pp.1–13 (2014)

(10) S. Chen, W. Chen, J. Liu, W. Chen, and Y. Jin: “Development of an aerostatic bearing system for roll-to-roll printed electronics”, *Journal of Micromechanics and Microengineering*, Vol.28, pp.1–14 (2018)

(11) X. Zhou, D. Wang, J. Wang, and S.C. Chen: “Precision design and control of a flexure-based roll-to-roll printing system”, *Precision Engineering*, Vol.45, pp.332–341 (2016)

(12) T. Atsumi, A. Okuyama, and M. Kobayashi: “Track-Following Control Using Resonant Filter in Hard Disk Drives”, *IEEE/ASME Transactions on Mechatronics*, Vol.12, No.4, pp.472–479 (2007)

Kenta Seki (Senior Member) received the B.S., M.S., and Dr.Eng. degrees in electrical and computer engineering from Nagoya Institute of Technology, Nagoya, Japan, in 2000, 2002 and 2009, respectively. From 2002 to 2006, he was with the Mechanical Engineering Research Laboratory, Hitachi, Ltd., Ibaraki, Japan. From March 2006, he joined a Research Associate with the Project Research Laboratory on Motion Systems, Nagoya Institute of Technology, Nagoya, Japan, where he is currently an Associate Professor with the Department of Electrical and Mechanical Engineering. His current research interests are the mechatronics system design and design of dynamically testing systems. Prof. Seki is a member of the Institute of Electrical Engineering of Japan, the Society of Instrument and Control Engineers, and the Japan Society of Mechanical Engineers.

Takayuki Kikuchi (Non-member) received the B.S. and M.S. degrees in electrical and mechanical engineering from Nagoya Institute of Technology, Nagoya, Japan, in 2016 and 2018. From 2018, he has been with the Sumitomo Heavy Industries, Ltd., Tokyo, Japan.

Makoto Iwasaki (Senior Member) received the B.S., M.S., and Dr.Eng. degrees in electrical and computer engineering from Nagoya Institute of Technology, Nagoya, Japan, in 1986, 1988, and 1991, respectively. Since 1991, he has been with the Department of Computer Science and Engineering, Nagoya Institute of Technology, where he is currently a Professor. His current research interests are the applications of control theories to linear/nonlinear modeling and precision positioning, through various collaborative research activities with industries. Prof. Iwasaki is a member of the Institute of Electrical Engineering of Japan and the Japan Society for Precision Engineering.